Journal of Statistical Physics, Vol. 56, Nos. 1/2, 1989

Bifurcations of a Lattice Gas Flow under External Forcing

Roberto Benzi[1] **and Sauro Succi**[2]

Received November 9, 1988; revision received January 27, 1989

We study the behavior of a Frisch–Hasslacher–Pomeau lattice gas automaton under the effect of a spatially periodic forcing. It is shown that the lattice gas dynamics reproduces the steady-state features of the bifurcation pattern predicted by a properly truncated model of the Navier–Stokes equations. In addition, we show that the dynamical evolution of the instabilities driving the bifurcation can be modeled by supplementing the truncated Navier–Stokes equation with a random force chosen on the basis of the automaton noise.

KEY WORDS: Lattice gas automata; turbulence; bifurcations; stochastic processes; Navier–Stokes equations.

1. INTRODUCTION

In the last few years there has been a growing interest in the study of lattice gas automata[1] (LGA) as a valuable tool to simulate two-dimensional and, more recently, also three-dimensional fluid flows.[2] This interest is motivated by at least two kind of reasons. One is that LGA may provide a practical breakthrough for simulating flows in complex geometries using massive parallelism on special-purpose computers.[3] The second is that LGA are an appealing tool for studying the whole set of scales of motion, ranging from "hydrodynamic fluctuations" up to large-scale coherent structures. LGA simulations have been successfully compared against experimental and numerical results for two- and three-dimensional flows at moderate Reynolds numbers. In LGA simulations the Reynolds number, or, equivalently, the viscosity can be estimated by means of the fluctuation-dissipation theorem.[7] Alternatively,[4] one can define the dissipative scale

[1] Department of Physics, Rome University "Tor Vergata," 00173, Rome, Italy.
[2] IBM/ECSEC, European Center for Scientific and Engineering Computing, Rome, Italy.

0022-4715/89/0700-0069$06.00/0

l_d in a fluid as the scale at which the microscopic noise becomes comparable to the hydrodynamic signal, and then compute the viscosity as $\nu \sim u_d l_d$, u_d being a typical velocity fluctuation at the scale l_d. Both ways show that there is an intimate connection between the microscopic noise and the dissipative effects taking place in a fluid.

This is only a particular aspect of a more general question which can be asked via LGA simulations, which concerns the effect of the microcospic noise on the hydrodynamic scales of motion. In the present paper we adress this question in a well-defined case. We consider a two-dimensional incompressible flow in a square box with periodic boundary conditions, forced by a large scale shear flow (see Section 3). Denoting by F the strength of the forcing term, we know that for small F the flow pattern is the same as the one of the forcing term. However, for F larger than a certain critical value F_c, according to well-known stability theorems established for two-dimensional shear flows, a bifurcation should occur. Then, for $F > F_c$ the flow develops a new pattern which differs from the one imposed by forcing term because of the contribution of the bifurcated modes. One can easily show that the amplitude of the bifurcated pattern depends on F, while the characteristic time of the onset of the bifurcation depends on the level of microscopic noise acting in the system as well as on the initial conditions. By the central manifold theorem, we know that a fluid system near the bifurcation threshold can be accurately described by a few degrees of freedom, and precisely those specifying the unstable manifold.[5] It follows that for F sufficiently close to F_c one can undertake an enlightening comparison between the stochastic LGA dynamics and the dynamics resulting from the projection of the Navier–Stokes equations, stochastically perturbed by the hydrodynamic noise, onto the unstable manifold. This comparison is the central focus of the present investigation. We show that the two stochastic dynamics exhibit a remarkable agreement once the stochastic noise, computed by measuring the variance of the forced pattern of the lattice gas in a subcritical regime, is included in the truncated Navier–Stokes equations.

The shear forcing has been chosen in the form of a spatially periodic profile, the so-called Kolmogorov flow, which implies that the corresponding Fourier amplitude can be used as a forcing parameter (for a review on the Kolmogorov flow see ref. 6). This choice also implies that the unstable manifold is of low codimensionality, namely 2, and can consequently be characterized by a small number of Fourier modes. Finally, we investigate the probability density distribution (p.d.d.) of the hydrodynamic fluctuations. It turns out that the p.d.d. is pretty close to a Gaussian, thus allowing us to assume that the stochastic noise acting in the system is essentially a white noise. Our results confirm the existence of a clear link

between LGA models and the mathematical theory of stochastic differential equations. We are currently investigating further connections between these two fields (for example, the presence of "large-deviations" effects).

2. THE MODEL

Our investigation is based upon the Frisch–Hasslacher–Pomeau (FHP) cellular automaton.[1] This automaton consists of a set of "pseudoparticles" which are constrained to move with a unit speed and a unit mass along the links of a hexagonal lattice. Hence, the state of the automaton is entirely specified in terms of a set of Boolean variables s_{ij} which take the value zero or one according to whether the jth site holds a particle moving along the ith link or not. The interaction between the pseudoparticles is governed by a set of collision rules which, site by site, mimic the momentum transfers occurring in a real fluid. These collision rules are subject to the constraint that, on each site, the particle number as well as the linear momentum must be conserved. In addition, collisions are compatible with an exclusion principle which forbids the simultaneous presence of two or more particles with the same speed at the same spatial location.

These simple prescriptions are sufficient to construct the microdynamic equations which govern the evolution of the Boolean field s_{ij}. Starting from the microdynamic equations and taking the appropriate limits described in ref. 7, it is possible to derive a set of macroscopic equations which govern the evolution of the hydrodynamic fields, such as the density and the velocity of the automaton "fluid." For low Mach number the macroscopic read as follows:

$$\nabla \cdot \mathbf{J} = 0 \tag{2.1}$$

$$\partial_t \mathbf{J} + [g(\rho)/\rho]\,\mathbf{J} \cdot \nabla \mathbf{J} = \nu\, \Delta \mathbf{J} - c_s^2\, \nabla \rho' \tag{2.2}$$

where ρ and $\mathbf{J}$ are the mass density and mass current density, respectively. The quantity ρ' represents the density perturbation with respect to the equilibrium value and $c_s = (3/7)^{1/2}$ is the (dimensionless) speed of sound of the automaton fluid. The coefficient ν is the kinematic shear viscosity and $g(d) = 7(2d-7)/12(d-1)$ is a characteristic advection-rescaling factor associated with the lack of Galilean invariance of the lattice and d the mean density per link. The macroscopic variables ρ and $\mathbf{J}$ should result upon ensemble averaging of the microdynamic equations which govern the evolution of the Boolean field of the automaton. In practice, they are defined as spatial (or spatiotemporal) averages over a subregion of the

lattice. In the present work, we use square blocks containing n sites per dimension, so that the macroscopic variables are defined as follows:

$$\rho = \sum_{i=1}^{7} \sum_{j=1}^{n^2} s_{ij}, \qquad \mathbf{J} = \sum_{i=1}^{7} \sum_{j=1}^{n^2} s_{ij} \mathbf{c}_i \tag{2.3}$$

where $\mathbf{c}_i$ $(i = 1, 7)$ is the set unit vectors connecting the jth site of the averaging box to its six nearest neighbors (conventionally we assume $\mathbf{c}_7 = \mathbf{0}$ for rest particles).[3]

We are interested in the behavior of the automaton under the effect of a spatially periodic force. For convenience, we assume this force to be directed along the horizontal direction x with a periodic dependence along the vertical coordinate y:

$$\mathbf{f}(y) = f_0 \sin(ky)\hat{\mathbf{x}} \tag{2.4}$$

where $\hat{x}$ is the unit vector along $\mathbf{x}$ and f_0 is a free parameter which will serve us to control the intensity of the forcing term. As described in ref. 7, the presence of such an additional term on the rhs of the Eq. (2.2) can be realized by introducing a bias in the collision rules which allows for reversal of the speed component along x, thus yielding a net momentum input along this direction. The spatial modulation of this net momentum input is obtained by allowing the extra collision to occur with a probability which is proportional to the prescribed shape factor $\sin(ky)$. As a result of the new automaton dynamics, Eq. (2.2) acquires an extra term $\rho f_0 \sin(ky)$ and reads therefore as follows:

$$\partial_t \mathbf{J} + [g(\rho)/\rho]\mathbf{J} \cdot \nabla \mathbf{J} = \nu \Delta \mathbf{J} - c_s^2 \nabla \rho' + \rho f_0 \sin(ky)\hat{\mathbf{x}} \tag{2.5}$$

When the forcing is "weak," and consequently the nonlinear term is "small" $(\mathbf{J} \cdot \nabla \mathbf{J} \ll \nu \Delta \mathbf{J})$, the physics contained in the above equation is controlled by the usual competition between the source, which feeds free energy into the system, and the collisional effects, which dissipate it. After a ramp up time of the order of $1/\nu k^2$, these two mechanisms balance each other and the current density attains a steady-state value $\rho f_0/\nu k^2$. However, when the forcing term becomes sufficiently large, nonlinear mode–mode coupling effects may be triggered which can alter the simple picture outlined above in a substantial way. It is therefore of interest to probe the automaton dynamics in this delicate and challenging scenario.

[3] Note that the averaging factor $1/n^2$ has been omitted in the definition of ρ and $\mathbf{J}$ given by Eq. (2.3). Consequently, ρ and $\mathbf{J}$ are to be interpreted as integral quantities associated with each macroscopic box.

3. STABILITY ANALYSIS

We find it convenient to recast Eq. (2.2) in terms of the stream function Ψ, defined by $\partial_x \Psi = -J_y$ and $\partial_y \Psi = J_x$. This reads:

$$\partial_t \Delta\Psi + \beta\{\Psi, \Delta\Psi\} = \nu\Delta\,\Delta\Psi - \alpha\Delta\,\Delta\Phi \tag{3.1}$$

where the symbol $\{\cdot, \cdot\}$ denotes the Jacobian, $\Phi = \cos(ky)$,

$$\alpha = \frac{\rho f_0}{k^3} \equiv 2F \tag{3.2}$$

and

$$\beta = \frac{g(\rho)}{\rho} \tag{3.3}$$

Our goal is to compare the automaton dynamics with the solution of Eq. (3.1). For small values of F we expect $\bar{\Psi} \equiv 2F\Phi/\nu$ to be a stable steady state, while for F greater than a critical value F_c this steady state becomes unstable. In order to compute F_c, we have to perform a linear stability analysis of Eq. (3.1) around the steady state $\bar{\Psi}$. This implies solving the following linear partial differential equation for the fluctuating component ψ of the stream function Ψ:

$$\partial_t \Delta\psi + \beta\psi_x \bar{\Psi}_{yyy} - \beta\bar{\Psi}_y \partial_x \Delta\psi = \nu\Delta\,\Delta\psi \tag{3.4}$$

This equation is solved in terms of normal modes

$$\psi = \exp(\lambda t)[A(y)\sin(mx) + B(y)\cos(mx)] \tag{3.5}$$

where each mode along x can be examined separately because the steady-state $\bar{\Psi}$ only depends on y. After Fourier expanding along y and retaining only first-order harmonics (which can be shown to be accurate within 2% for $m = 1$), one obtains

$$F_c = \inf_m \left\{ \nu^2 \frac{m^2 + k^2}{\beta k (k^2 - m^2)^{1/2}} \right\} = \frac{\nu^2(1 + k^2)}{\beta k (k^2 - 1)^{1/2}} \tag{3.6}$$

where $k = 0, \sigma, 2\sigma, \ldots$, with σ the aspect ratio of the rectangular domain, namely $2/\sqrt{3}$. It should be noted that since the forcing depends only on one spatial coordinate, the two eigenvalues coincide: hence the unstable manifold has codimension 2.

For $F \sim F_c$ we expect the dynamics of the Navier–Stokes equations to be dominated by the unstable modes $(m = 0, k)$, $(m = 1,\ k = 0)$, and

$(m=1, k)$, to which all the others become rapidly "slaved." The resulting reduction in the number of effective degrees of freedom can be exploited to express the stream function ψ solely in terms of the triplet of unstable modes, that is, by assuming

$$\psi = A_{10}\exp(ix) + A_{1k}\exp(ix+iky) + A_{0k}\exp(iky) + (*) \tag{3.7}$$

Inserting this expression in (2.4), we obtain the following equations of motion for the amplitudes A_{10}, A_{1k}, and A_{0k}:

$$k^2\dot{A}_{0k} + \nu k^4 A_{0k} - k^4 F = -\beta k^3 A_{10}^* A_{1k} \tag{3.8}$$

$$\dot{A}_{10} + \nu A_{10} = \beta k A_{0k}^* A_{1k} \tag{3.9}$$

$$(1+k^2)\,\dot{A}_{1k} + \nu(1+k^2)^2\,A_{1k} = \beta k(k^2-1)\,A_{0k}A_{10} \tag{3.10}$$

For $F > F_c$, the stable steady-state solution of Eqs. (3.8)–(3.10) reads

$$\begin{aligned} \tilde{A}_{0k} &= F_c/\nu \\ \tilde{A}_{10} &= (k/\nu)\,F_c(F/F_c-1)^{1/2}\exp(i\theta) \\ \tilde{A}_{1k} &= (\nu/\beta)(F/F_c-1)^{1/2}\exp(i\theta) \end{aligned} \tag{3.11}$$

where $\exp(i\theta)$ is an arbitrary phase factor which results from the fact that the forcing does not depend on the x coordinate. In the following we shall directly compare the automaton dynamics with the solutions of Eqs. (3.8)–(3.10), stochastically perturbed by a random noise derived from the automaton dynamics (see next section).

In order to compare with the numerical result, it is useful to reexpress the criticality condition in terms of the *experimental* parameter $\dot{J}_t$, which represents the number of units of momentum injected per time step in the overall automaton along the horizontal direction. The link between $\dot{J}_t$ and f_0 is obtained by computing the total momentum change due to the force as

$$\dot{J}_t = \sum_{I=1}^{M^2} \rho\,\partial_t U = C\rho_0 f_0 n^2 \sum_{I=1}^{M^2} |\sin ky| \sim 2\frac{C}{\pi} N^2 \rho_0 f_0 \tag{3.12}$$

where N is the number of automata sites per dimension and $M = N/n$ is the number of averaging boxes per dimension used to define the fluid fields and $\rho_0 = \rho/n^2$. In this equation C is a calibration coefficient, to be determined by the numerical experiment, which accounts for the marginal excitation of "satellite" harmonics besides the "pump" mode, due to the random nature of the implementation of the forcing term. Hence, a value of the coefficient

$C > 1$ should be expected. Combining Eqs. (3.7) and (3.12), we can finally compute the critical value $\dot{J}_{tc}$ as

$$\dot{J}_{tc} = 32C\pi^2\rho_0 v^2 \frac{k^2}{gN} \frac{m^2 + k^2}{(k^2 - m^2)^{1/2}} \tag{3.13}$$

This formula serve us as a guideline to compare the numerical results with the predictions of the truncated Navier–Stokes model (see next section).

4. NUMERICAL RESULTS

In order to test the behavior of the FHP automaton with respect to the theoretical predictions of the reduced NS model, we have performed a series of numerical experiments with an in-core Fortran code running on a IBM 3090 with vector facility at a processing rate of 0.1 CPU sec per time step.[9] The automaton consists of 1024^2 grid points equally distributed in a rectangular domain of side 2π along x and $3^{1/2}\pi$ along y with a cell density $d \equiv \rho/7n^2 = 0.1$ and a null macroscopic initial current $\mathbf{J} = 0$. Spatial averaging is performed over blocks of 16^2 automaton sites, so that the macroscopic variables are defined over a 64^2 grid. The forcing term has the form given by Eq. (2.4) with a pump wavenumber $k = 3\sigma$.

To help the clarity of the discussion of the numerical results, a few words on the implementation of the periodic force are in order. In order to profit from multispin coding, the state of the automaton has been encoded into a series of seven arrays of dimension N along y and $N/32$ along x, 32 being the number of bits in a single computer word. Therefore, we find it convenient to regard the computational domain as a collection of $N_b = (N/32)^2$ nonoverlapping boxes, each containing 32^2 spatial locations. At each time step, a prescribed fraction, say f, of these N_b boxes is elected for momentum input along x. This means that once a given box and a given site within this box have been identified (at random), a random number r between -1 and 1 is extracted and compared with a local estimator $e = \sin ky$. The procedure is now as follows:

If $|e| < r$: process another box (if any).

Else: construct a forcing operator O_f and apply it in addition to the usual momentum-conserving operator.

This forcing operator has been chosen such as to transfer quanta of momentum from directions $3 \to 2$, $4 \to 1$, and $5 \to 6$ if $\sin ky > 0$ and vice versa if $\sin ky < 0$ (links are labeled 1 to 6 counterclockwise, with 1 corresponding to propagation along $+x$). Clearly, O_f reduces to the identity whenever the state of the automaton at that given site does not allow for

the transitions mentioned above. For instance, if link 3 is empty and link 2 is occupied, no transfer of positive quanta from 3 to 2 can take place.

As a result, each site can receive a momentum input along x ranging from 0 to 4 units, so that the global momentum input rate $\dot{J}_t$ ranges from zero to $4fN_b d(1-d)$, the factor $d(1-d)$ being related to the binary nature of O_f. This upper bound guides the choice of f to obtain values of $\dot{J}_t$ in the desired range (sub or supercritical).

Let us now come to the illustration of the numerical results. In a linear regime, the steady-state amplitude of the mass current J_{03} is related to the forcing parameter f_0 by the relation $J_{03} = \rho f_0 / \nu k_a^2$, where $k_a = 2\pi k/N$ is the pump wavevector in automata units. Due to Eqs. (3.12), this relation can also be written as

$$\bar{J}_{03} \equiv \frac{J_{03}}{n^2} = \frac{\dot{J}_t}{C 8\pi \nu k^2} \tag{4.1}$$

This expression refers to a nonbifurcated linear response and consequently we have to check it in a subcritical ($F < F_c$) regime. According to the expression (3.13), if we assume $C = 1$ (full control over the force strength), the critical momentum input for the wavenumber ($m = 0$, $k = 3\sigma$) is $\dot{J}_{tc} \sim 1.95$. In order to be reasonably sure of running below the critical threshold, we have chosen $\dot{J}_t \sim 0.67$.

Consistent with this choice, the numerical experiment does not exhibit any bifurcation, the only harmonic excited in the spectrum being the original one $(0, 3\sigma)$, as it is apparent from Fig. 1, which displays the automaton flow after 300×1024 steps. The experimental value of the amplitude of this harmonic is $|\bar{J}_{03}| = 6 \times 10^{-3}$, which is matched to the theoretical value of 6.6×10^{-3} by fixing $C \sim 1.1$ in Eq. (3.13). This raises the "effective" critical threshold to about $J_{tc} \sim 2.1$, which, being fairly above the experimental value of 0.67, proves the consistency of the subcritical experiment.

Having calibrated the forcing term, we can proceed to probe the automaton in the more challenging supercritical regime. To this purpose we choose $\dot{J}_t = 2.6$. In this case, after the initial onset of the linear mode, the automaton displays a neat bifurcation which becomes manifest through the appearance of the modes $(1, 0)$ and $(1, 3\sigma)$. The existence of these modes is clearly detectable in Fig. 2, which shows the velocity field of the automaton after 400×1024 steps. Along the vertical direction we recognize three wavelengths due to the linear mode, interspersed with "islands" which are the signature of the bifurcated $(1, 0)$ mode. This qualitative agreement can be checked quantitatively by measuring the steady-state amplitudes of the three interacting modes. The experiment yields $|\bar{J}_{03}| \sim 1.8 \times 10^{-2}$, $|\bar{J}_{10}| \sim 10^{-2}$, and $|\bar{J}_{13}| \sim 5.6 \times 10^{-3}$ to be compared with the theoretical

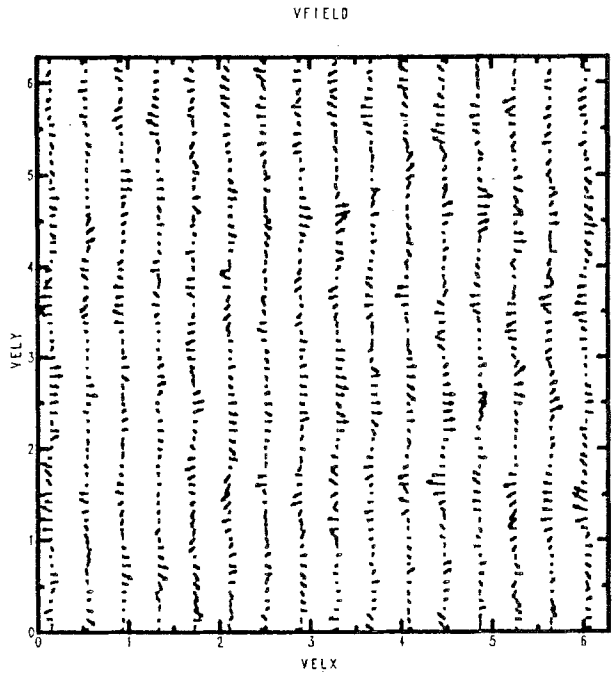

Fig. 1. The flow pattern in the subcritical regime $F < F_c$, $\dot{J}_t = 0.67$. Note the modulation of the velocity field corresponding to the pump mode $(0, 3\sigma)$.

values given by Eqs. (4.1) and (3.11), which are 2×10^{-2}, 9×10^{-3}, and 8×10^{-3}, respectively. We note that there is about a 15% discrepancy between the theoretical values and those obtained by the automaton. However, by taking into account further degrees of freedom [i.e., mode $(2, 3\sigma)$, which is directly excited by the nonlinear coupling of modes $(1, 3\sigma)$ and $(1, 0)$], this discrepancy reduces to roughly 5%.

These results indicate that the steady-state hydrodynamic behavior of the automaton under a periodic forcing reproduces the one predicted by the truncated Navier–Stokes equations with a reasonable accuracy.

The same consideration does *not* apply to the dynamics of the bifurcation, which, in the case of the automaton is greatly affected by the presence of the "molecular noise," a feature which has no counterpart in the Navier–Stokes picture. On intuitive grounds, one expects the main effect of the molecular noise to be an anticipation of the onset of the instability. In order to investigate this point, we introduce a stochastic version of the reduced Navier–Stokes model which includes a random forcing term tailored on the basis of the automaton noise. From the analysis presented in ref. 7, we know that, by neglecting nonlinear terms, the automaton noise

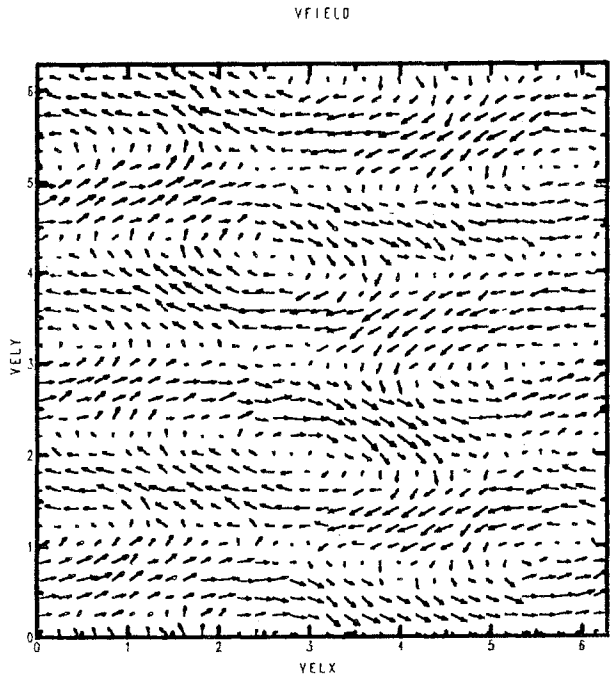

Fig. 2. The flow pattern for $\dot{J}_t = 2.6$, i.e., in a supercritical regime. One recognizes the presence of the bifurcated modes which produce the roll-like structures.

produces the same variance on each Fourier mode of the velocity field. This implies that the stochastic (Langevin) version of Eqs. (3.8)–(3.10) reads

$$d[k^2 a_1] = [-\nu k^4 a_1 - Fk^4 - \beta k^3 (a_2 a_4 + a_3 a_5)]\, dt + \varepsilon^{1/2} k^2\, dW_1 \tag{4.2}$$

$$d[k^2 b_1] = [-\nu k^4 b_1 - \beta k^3 (a_2 a_5 - a_3 a_4)]\, dt + \varepsilon^{1/2} k^2\, dW_2 \tag{4.3}$$

$$d[a_2] = [-\nu a_2 + \beta k a_4 a_1]\, dt + \varepsilon^{1/2}\, dW_3 \tag{4.4}$$

$$d[a_3] = [-\nu a_3 + \beta k a_5 a_1]\, dt + \varepsilon^{1/2}\, dW_4 \tag{4.5}$$

$$d[(k^2+1)\, a_4] = [-\nu (k^2+1)^2\, a_4 + \beta k (k^2-1)\, a_1 a_2]\, dt + \varepsilon^{1/2} (k^2+1)\, dW_5 \tag{4.6}$$

$$d[(k^2+1)\, a_5] = [-\nu (k^2+1)^2\, a_5 + \beta k (k^2-1)\, a_1 a_3]\, dt + \varepsilon^{1/2} (k^2+1)\, dW_6 \tag{4.7}$$

where $A_{0k} = a_1 + ib_1$, $A_{10} = a_2 + ia_3$, $A_{1k} = a_4 + ia_5$, and dW_j is a Wiener noise of zero mean and variance dt. Of course, this set of stochastic equations is meaningful only if the automaton noise is indeed of Gaussian type.

To check this point, we have analyzed the velocity signal produced by the automaton in the subcritical case and assessed its basic statistical properties. This analysis has led us to conclude that the automaton noise is quite close to a Gaussian noise, its amplitude ε being about 60 for the specific case under consideration, a value about two times smaller than the theoretical predictions based upon the fluctuation-dissipation theorem. We have performed a series of companion simulations of the reduced NS system in both its deterministic and stochastic versions. A synthetic picture of the results of these simulations is shown in Fig. 3, where we report the time evolution of the bifurcated mode (1, 0) as obtained by the original automaton (label A), the deterministic Navier–Stokes model (solid line), and its stochastic version (dotted line). This figure confirms a reasonable agreement between the steady-state amplitudes of the modes in all three kinds of models: automaton, deterministic, and stochastic Navier–Stokes. The dynamic behavior of the stochastic models, both the automaton and the Navier–Stokes, displays, however, a striking anticipation of the onset of the instability. As already mentioned, this anticipation matches the physical intuition that by increasing the amount of fluctuations, the system tends to be driven away from the unstable state more and more rapidly. To judge the effect of the noise amplitude on the escape time of the system, we have

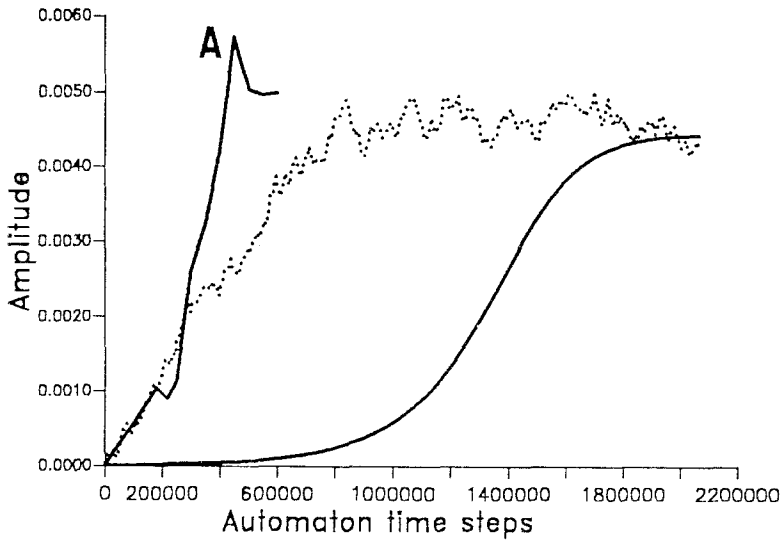

Fig. 3. The amplitude of the current density **J** for the mode (1, 0) as a function of time. The label A refers to the automata simulation, the solid line to the deterministic Navier–Stokes integration, and the dotted line to the Navier–Stokes integration stochastically perturbed. On the horizontal axis units refer to automata time steps.

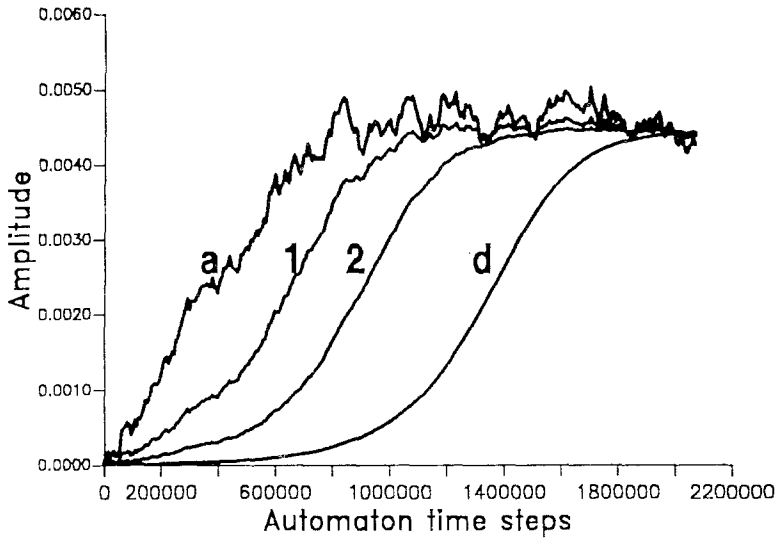

Fig. 4. Amplitude of the current density for the mode (1, 0) obtained by numerically integrating the stochastically perturbed Navier–Stokes equation for different values of the noise intensity. Labels *a*, 1, 2, and *d* refer to different intensities of the noise ε, namely *a* to $\varepsilon = 60$ (the value used in the computations of Fig. 3), 1 to $\varepsilon = 6$, 2 to $\varepsilon = 0.6$, and *d* to $\varepsilon = 0$, i.e., the deterministic evolution.

run the Langevin simulation with four different values of ε, namely 0, 0.6, 6, and 60. The results are displayed in Fig. 4. This figure shows that the onset time of the instability is a sensitive function of the noise amplitude and proves therefore that the agreement between the Langevin simulations and the automata dynamics is not incidental but results from an appropriate choice of the noise level. Since the noise level is essentially controlled by the spatial resolution, it is clear that LGA simulations offer the opportunity of using the lattice spacing as a "handle" to tune the noise strength and accomplish a systematic study of the transition from strongly fluctuating to hydrodynamic Navier–Stokes regimes.

5. CONCLUSION

We have shown that the FHP lattice gas dynamics correctly reproduces the steady-state features of the bifurcated regime of a Navier–Stokes fluid under the effect of a spatially periodic force. However, an important difference in the dynamical behavior has also been pointed out. This concerns a considerable anticipation of the onset of the instability which leads to the bifurcation. We have also shown that the same effect can

be detected within the framework of a stochastic (Langevin) formulation of the reduced Navier–Stokes model. This proves that there is a clear link between LGA dynamics and the theory of stochastic differential equations.[10] It seems therefore reasonable to expect that further investigations along this line will deepen our understanding of the fluid behavior in the presence of random fluctuations and, ultimately, of the mechanisms which govern dissipative phenomena in fluid systems.

ACKNOWLEDGMENTS

We thank Dr. D. d'Humieres for pointing out the scale factor $\sqrt{3}/2$ along the vertical direction which had been overlooked in a previous version of this manuscript.

REFERENCES

1. U. Frisch, K. Hasslacher, and Y. Pomeau, *Phys. Rev. Lett.* **56**:1065 (1986).
2. J. P. Rivet, M. Henon, U. Frisch, and D. d'Humieres, *Europhys. Lett.* **7**:231 (1988).
3. N. Margolus, T. Toffoli, and G. Vichniac, *Phys. Rev. Lett.* **56**:1694 (1986).
4. S. Succi, P. Santangelo, and R. Benzi, *Phys. Rev. Lett.* **27**:2739 (1988).
5. J. Marsden and M. McCracken, *The Hopf Bifurcation and Its Applications* (Springer, Berlin, 1976).
6. Zhen-su-She, Instabilités et Dynamique a Grande Echelle en Turbulence, Ph.D. Thesis, Université de Paris VII (1987).
7. U. Frisch, D. d'Humieres, B. Hasslacher, P. Lallemand, Y. Pomeau, and J. P. Rivet, *Complex Systems* **1**:649 (1987).
8. E. Knobloch and I. Guckenheimer, *Phys. Rev. A* **27**:408 (1983).
9. S. Succi, *Comp. Phys. Commun.* **47**:173 (1987).
10. D. Ludwig, *SIAM Rev.* **17**:605 (1975).